Shape Distributions for Gaussian Molecules: Circular and Linear Chains as Spheres and Ellipsoids of Revolution

Gaoyuan Wei and B. E. Eichinger*

Department of Chemistry, BG-10, University of Washington, Seattle, Washington 98195.
Received December 5, 1988; Revised Manuscript Received February 2, 1989

ABSTRACT: Shape distribution functions, i.e., probability distributions of the principal components of the gyration tensor, for Gaussian molecules in three-dimensional space have been numerically evaluated for circular and linear chains as spheres and ellipsoids of revolution. For spherical configurations, the three principal components of the gyration tensor are equal, while two of the principal components are identical in the space of ellipsoidial configurations. These configurations lie on the boundary of the domain of all possible ellipsoids. As in two dimensions, the most probable configurations in three dimensions are very compact when compared to the mean-square dimensions of general ellipsoids. For ellipsoids of revolution, fluctuations away from the most probable configurations are found to be highly asymmetric; their distribution functions consist of two parts: prolate and oblate. Gaussian molecules are, on the average, more likely to be prolate than oblate, with the prolate-to-oblate probability ratio being 3.33:1 and 6.31:1 for circular and linear chains with 61 Rouse beads, respectively. These results complete the description of symmetric configurations in three-dimensional space.

Introduction

The need to determine shape distributions for macroscopic random elastic networks has motivated this study of the distributions for individual macromolecules.[1,2] The earlier results obtained by Šolc, Stockmayer, and Gobush on the shape distributions for long linear chains in three-dimensional space and circular chains in two dimensions revealed many interesting features of the distributions, such as their large asymmetry.[3-6] Later, a general treatment of this problem was borrowed from the theory of multivariate statistics by one of us, thus providing a complete formal solution to the problem.[7,8] Apart from the relatively simple asymptotic formulas,[9] the formal solution as a series in zonal polynomials is practically useless for polymer scientists who wish to gain some insight into the behavior of macromolecules. More tractable results are obtained when the integrals are formulated in Fourier space, with the last few integrals being left for numerical evaluation. These numerical computations were done for circular and linear chains as disks and ellipses in two-dimensional space, and the plots displayed detailed information about the shape distributions.[10] Another effort to describe the shape of macromolecules is that of Theodorou and Suter.[11] They computed segment density distributions for a rotational isomeric state model of polypropylene by Monte Carlo techniques. Their results show that chains are highly anisometric. More recently, various analytical and Monte Carlo results were obtained for shape parameters of polymers as unrestricted or restricted, open or closed random walks.[12-17]

We have completed the numerical evaluations of the shape distribution functions for circular and linear chains of two different lengths for the subset of configurations in which the chains are spheres and ellipsoids of revolutions. These distributions provide considerable insight into the quantitative features of the shape of Gaussian molecules, and the techniques used to evaluate them will be of use in applications to rubber elasticity. In the following, the general shape distribution functions are first reduced to computationally tractable forms. Then we focus on the distributions for circular and linear chains as spheres, obtaining both analytical and numerical results. Immediately following that is the treatment of the distribution functions for the same types of molecules as ellipsoids of revolution, with a few complicated but useful equations and several plots for the distribution functions displayed. Finally the numerical results obtained for both spheres and ellipsoids of revolution are discussed.

General Formulation

For a system of n identical particles imbedded in a k-dimensional space, the gyration tensor $\mathbf{S}$ takes the form

$$\mathbf{S} = n^{-1}\mathbf{X}\mathbf{X}' \tag{1}$$

where $\mathbf{X}$ is a $k \times n$ matrix of coordinates in an arbitrarily oriented coordinate frame with origin at the center of mass and $\mathbf{X}'$ is the transpose of $\mathbf{X}$. In the framework of the Gaussian model the effective potential of mean force is $\beta V(\mathbf{X}) = \mathrm{tr}\,(\mathbf{X}\mathbf{K}_\gamma\mathbf{X}')$, where $\mathbf{K}_\gamma$ is the Kirchhoff matrix that describes the connectivity of the molecule. The shape distribution function is readily formulated in normal coordinates $\mathbf{Q}_0$ and is given by[8]

$$P(\mathbf{S})\,d\mathbf{S} = (d\mathbf{S}/Z)\int \mathrm{etr}\,(-\mathbf{Q}_0\Lambda_\gamma\mathbf{Q}_0')\,d\mathbf{Q}_0/d\mathbf{S} \tag{2}$$

where Z is a normalization constant. For a molecule of n Rouse beads with a mean-square segment length $\langle l^2\rangle_0$, the diagonal matrix $\Lambda_\gamma = \mathrm{diag}\,(\gamma\lambda_1,\gamma\lambda_2,...,\gamma\lambda_{n-1})$ consists of the nonzero eigenvalues of $\mathbf{K}_\gamma$, with $\gamma = k/2\langle l^2\rangle_0$. The next step is to express eq 2 in Eckart coordinates through the polar decomposition $\mathbf{Q}_0 = n^{1/2}\mathbf{h}\mathbf{S}_d^{1/2}\mathbf{V}$, where $\mathbf{h} \in \mathbf{SO}(k)$ [$\mathbf{SO}(k)$ is the special orthogonal group acting on a k-dimensional space], $\mathbf{S}_d$ is the diagonal matrix of the principal components of the gyration tensor, and $\mathbf{V} = \mathbf{V}_{k,n-1}$ is a $k \times (n-1)$ matrix with $\mathbf{V}\mathbf{V}' = \mathbf{1}_k$. The space $\mathbf{V}$ is a Stiefel manifold.[9]

To formulate $P(\mathbf{S})\,d\mathbf{S}$ in Eckart coordinates, use is made of the metric on the $k(n-1)$-dimensional normal mode space $\mathbf{Q}_0$, from which the volume element $d\mathbf{Q}_0$ is obtained.[7-10] In so doing, eq 2 becomes

$$P(\tilde{\mathbf{S}}_d)\,d\tilde{\mathbf{S}}_d = (d\tilde{\mathbf{S}}_d/Z_p)E(\tilde{\mathbf{S}}_d)\int_{\mathbf{V}\mathbf{V}'=\mathbf{1}} \mathrm{etr}\,(-\tilde{\mathbf{S}}_d\mathbf{V}\kappa\mathbf{V}')\,d\mathbf{V} \tag{3}$$

where $p \le k$ designates the number of unequal principal components of the gyration tensor, $\tilde{\mathbf{S}}_d = \gamma\mathbf{S}_d/n$ is the diagonal matrix of the reduced principal components, $d\tilde{\mathbf{S}}_d$ is defined as the differential volume of the unequal reduced principal components, $\kappa = \mathrm{diag}\,(\kappa_1,\kappa_2,...,\kappa_{n-1})$ with $\kappa_j = n^2\lambda_j$, Z_p is a normalization constant, and $E(\tilde{\mathbf{S}}_d)$ is a function of the reduced principal components only, which, as a part of the volume element $d\mathbf{Q}_0$, may be written down for any given p. For $p = k$, eq 3 was solved analytically, with the result expressible in terms of the two-matrix hypergeometric function.[8,9] For spherically symmetric configurations, where $\tilde{\mathbf{S}}_d = \tilde{S}\mathbf{1}_k$, the function $E(\tilde{\mathbf{S}}_d)$ is

$$E(\tilde{\mathbf{S}}_d) = \tilde{S}^{[kn-k(k-3)/2-1]/2} \tag{4}$$

0024-9297/89/2222-3429$01.50/0

Table I
Definitions of $\tilde{\mathbf{S}}_d$ and $B(\tilde{\mathbf{S}}_d)$ for 3-D Shape Distributions

$\tilde{\mathbf{S}}_d$	$B(\tilde{\mathbf{S}}_d)$
$(\tilde{S}, \tilde{S}, \tilde{S})$	$\tilde{S}^{5/2}$
$(\tilde{S}_\perp, \tilde{S}_\perp, \tilde{S}_\parallel)$	$\tilde{S}_\perp(\tilde{S}_\parallel - \tilde{S}_\perp)^2$
$(\tilde{S}_1, \tilde{S}_2, \tilde{S}_3)$	$\lvert\tilde{S}_1 - \tilde{S}_2\rvert\lvert\tilde{S}_2 - \tilde{S}_3\rvert\lvert\tilde{S}_3 - \tilde{S}_1\rvert$

while for ellipsoids of revolution, where $\tilde{\mathbf{S}}_d = \text{diag}\,(\tilde{S}_\perp, \tilde{S}_\perp, \tilde{S}_\parallel)$, $E(\tilde{\mathbf{S}}_d)$ is given by

$$E(\tilde{\mathbf{S}}_d) = \tilde{S}_\parallel^{(n-5)/2}\tilde{S}_\perp^{n-4}(\tilde{S}_\parallel - \tilde{S}_\perp)^2 \quad (5)$$

Before attempting numerical evaluation of eq 3, it is necessary to reduce it to a more manageable form. This is accomplished with the use of δ functions to remove the constraint $\mathbf{VV}' = 1$, to yield

$$P(\tilde{\mathbf{S}}_d)\,d\tilde{\mathbf{S}}_d = (d\tilde{\mathbf{S}}_d/Z_p)B(\tilde{\mathbf{S}}_d)\int \text{etr}\,(i\tilde{\mathbf{S}}_d\mathbf{hxh}')\prod_{\alpha<\beta}^{k}|x_\alpha - x_\beta|\mathbf{1}_k \otimes \kappa_{n-1} + i\mathbf{x}_k \otimes \mathbf{1}_{n-1}|^{-1/2}\,d\mathbf{h}\prod_{\sigma=1}^{k}dx_\sigma \quad (6)$$

where Z_p is a new normalization constant, $\mathbf{h} \in \mathbf{SO}(k)$, $\mathbf{x} = \text{diag}\,(x_1, x_2, \ldots, x_k)$, the function $B(\tilde{\mathbf{S}}_d)$ is defined as

$$B(\tilde{\mathbf{S}}_d) = |\tilde{\mathbf{S}}_d|^{(k-n+2)/2}E(\tilde{\mathbf{S}}_d) \quad (7)$$

and the integration ranges are $-\infty \le x_k \le x_{k-1} \le \ldots \le x_1 \le \infty$. For $k = 3$, it is convenient to make a change of variables to $t = x_2$, $x = x_1 - x_2$, and $y = x_2 - x_3$; eq 6 may then be written in terms of the new variables t, x, and y as

$$P(\tilde{\mathbf{S}}_d)\,d\tilde{\mathbf{S}}_d = (d\tilde{\mathbf{S}}_d/Z_p)B(\tilde{\mathbf{S}}_d)\int_{-\infty}^{\infty}dt\int_0^\infty dx\int_0^\infty dy \int_{-1}^{1}dr\int_0^{2\pi}d\alpha\int_0^{2\pi}d\beta\; xy(x+y)F_1(t+x)F_2(t)F_3(t-y) \quad (8)$$

where Z_p is another normalization constant and the function $F_\mu(x)$ is defined as

$$F_\mu(x) = \exp(ixA_\mu)\prod_{j=1}^{n-1}(\kappa_j + ix)^{-1/2} \quad (9)$$

with $A_\mu = \sum_{\sigma=1}^{3}\tilde{S}_\sigma h_{\sigma\mu}^2$. In eq 8 the representation

$$\mathbf{h} = \begin{pmatrix} c_\alpha & s_\alpha & 0 \\ -s_\alpha & c_\alpha & 0 \\ 0 & 0 & 1 \end{pmatrix}\begin{pmatrix} 1 & 0 & 0 \\ 0 & c_\gamma & s_\gamma \\ 0 & -s_\gamma & c_\gamma \end{pmatrix}\begin{pmatrix} c_\beta & s_\beta & 0 \\ -s_\beta & c_\beta & 0 \\ 0 & 0 & 1 \end{pmatrix} \quad (10)$$

has been chosen, where $c_\alpha = \cos\alpha$, $s_\alpha = \sin\alpha$, and $-\cos\gamma = r$. The subscript p in Z_p takes the value 1 for spheres, 2 for ellipsoids of revolution, and 3 for general ellipsoids. The functions $B(\tilde{\mathbf{S}}_d)$ for these three cases are defined in Table I.

Spheres

For spherical molecules, $A_\mu = \tilde{S}$ for all μ. We therefore obtain from eq 8 the distribution function as

$$P(\tilde{S})\,d\tilde{S} = d\tilde{S}\,(8\pi^2/Z_1)\tilde{S}^{5/2}\int_{-\infty}^{\infty}dt\int_0^\infty dx\int_0^\infty dy\; xy(x+y)F(t+x)F(t)F(t-y) \quad (11)$$

where $F(x)$ is defined as

$$F(x) = \exp(ix\tilde{S})\prod_{j=1}^{n-1}(\kappa_j + ix)^{-1/2} \quad (12)$$

We now ask the following question: Is there a way to extend the integration limits of one of the two semiinfinite integrals to $(-\infty, \infty)$ so as to make use of the residue theorem more than once? Fortunately, the answer turns out to be positive. The trick is to note the integral identity

$$\int_0^\infty dx\int_0^\infty dy\; xy(x-y)F(t+x)F(t+y) = 0 \quad (13)$$

which holds for arbitrary t. This gives

$$P(\tilde{S})\,d\tilde{S} = d\tilde{S}\,(8\pi^2/Z_1)\tilde{S}^{5/2}\int_{-\infty}^{\infty}dt\int_{-\infty}^{\infty}dy\int_0^\infty dx\; xy(x+y)F(t+x)F(t)F(t-y) \quad (14)$$

In what follows, analytical results are presented for two types of molecules—linear and circular chains—both with an odd number of beads. For even n, the final equations appear slightly different from those for odd n, but the techniques employed to evaluate them are essentially the same. The $n = 5$ case is treated separately. The equations given below therefore hold for n greater than 5.

The double degeneracy of the eigenvalues $\kappa_j = 4n^2\sin^2(\pi j/n)$ for circular chains[8] allows one to carry out the two infinite integrals by use of the residue theorem twice, with the result

$$P(\tilde{S})\,d\tilde{S} = (d\tilde{S}/Z_C)\tilde{S}^{5/2}\sum_{j\neq k\neq l}^{(n-1)/2}(-1)^{j+k+l}(\kappa_k - \kappa_j)(\kappa_l - \kappa_j)\times (\kappa_k - \kappa_l)B_jB_kB_l\int_0^\infty \frac{\exp[-\tilde{S}(\kappa_j + 2\kappa_k + i\beta)]}{\beta + i(\kappa_l - \kappa_k)}\,d\beta \quad (15)$$

where B_j is defined by

$$B_j = \kappa_j/\prod_{l\neq j}^{(n-1)/2}|1 - \kappa_j/\kappa_l| \quad (16)$$

and Z_C is a normalization constant which may be evaluated through

$$\int_0^\infty P(\tilde{S})\,d\tilde{S} = 1 \quad (17)$$

One notices that the integral in eq 15 can be expressed in terms of the exponential-integral function of real argument.[18]

For linear chains, for which $\kappa_j = 4n^2\sin^2(\pi j/2n)$,[8] the existence of branch points requires evaluation of the integrals along proper branch cuts. Here we choose vertical branch cuts[19] for both infinite integrals. The result is

$$P(\tilde{S})\,d\tilde{S} = (d\tilde{S}/Z_L)\tilde{S}^{5/2}\int_0^\infty d\beta\int_0^{\pi/2}d\theta\int_0^{\pi/2}d\varphi\;\beta\sum_{j,k=1}^{(n-1)/2}(-1)^{j+k}(\epsilon_k - \epsilon_j)D_jD_k\exp[-\tilde{S}(\epsilon_j + 2\epsilon_k - i\beta)](\epsilon_j - \epsilon_k + i\beta)\prod_{l=1}^{n-2}(\kappa_l - \epsilon_k + i\beta)^{-1/2} \quad (18)$$

where $\epsilon_j = \kappa_{2j-1} + (\kappa_{2j} - \kappa_{2j-1})\sin^2\theta$, D_j is defined as

$$D_j = (\kappa_{2j}\kappa_{2j-1})^{1/2}\prod_{l\neq 2j,2j-1}^{n-1}|\epsilon_j/\kappa_l - 1|^{-1/2} \quad (19)$$

and Z_L is a normalization constant which, like Z_C, has an analytic solution.

For $n = 5$, a simple analytic solution to the distribution function for circular chains exists and is given by

$$P(\tilde{S})\,d\tilde{S} = (d\tilde{S}/3\pi^{1/2})(8/\chi_{5/2})\tilde{S}^{3/2}\exp(-3\kappa_+\tilde{S})\cosh(\kappa_-\tilde{S}) \quad (20)$$

where $\kappa_\pm = (\kappa_1 \pm \kappa_2)/2$. The function χ_α is defined as

$$\chi_\alpha = (\kappa_1 + 2\kappa_2)^{-\alpha} + (\kappa_2 + 2\kappa_1)^{-\alpha} \quad (21)$$

Table II
Most Probable Configurations (Spheres)

n	$*\tilde{S}$	$P(*\tilde{S})$	$\langle\tilde{S}\rangle$
		Circular	
5	0.0085	53.8089	0.0144
11	0.0185	59.3138	0.0217
61	0.0180	72.2465	0.0208
63	0.0175	72.2761	0.0208
99	0.0175	72.5661	0.0207
		Linear	
11	0.0225	45.3571	0.0271
25	0.0215	51.6058	0.0262
61	0.0215	52.9544	0.0262
99	0.0215	53.1076	0.0261

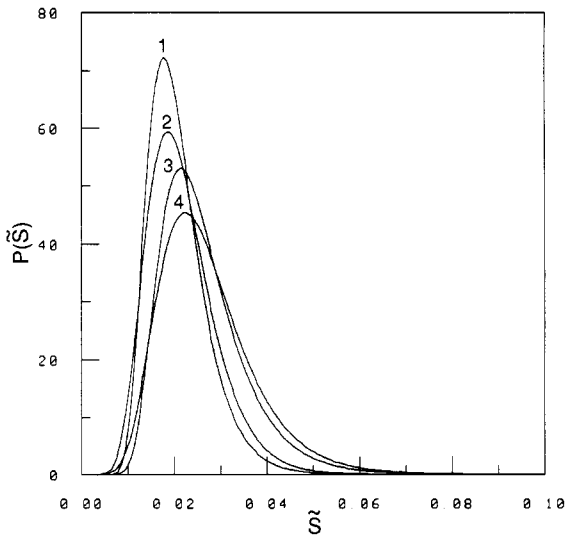

Figure 1. Size distribution $P(\tilde{S})$ for spherical configurations. Curves 1 and 2 are for circular chains with 61 and 11 beads, respectively, while curves 3 and 4 correspond to n = 61 and 11, respectively, for linear chains.

The first moment $\langle\tilde{S}\rangle$ may be expressed in terms of κ_1 and κ_2 as

$$\langle\tilde{S}\rangle = (5/2)\chi_{7/2}/\chi_{5/2} \tag{22}$$

whose numerical value, together with the most probable $\tilde{S}$, denoted by $*\tilde{S}$, and the value of the distribution function evaluated at $\tilde{S} = *\tilde{S}$, $P(*\tilde{S})$, is given in Table II.

In the numerical evaluation of eq 15 and 18, oscillating integrands are avoided by use of an exponentially scaled exponential-integral function to represent the Fourier integral in eq 15. The semiinfinite integral in eq 18 is transformed to a simpler one with a real-valued integrand by integrating along the imaginary axis of the complex plane where the branch points lie. The IMSL subroutine MMDEI[20] was used for calculating the exponential-integral function. All integrals were evaluated by use of Romberg integrators.[21]

Numerical computations on $P(\tilde{S})$ for a wide range of values of $\tilde{S}$ were done for three choices of n: 11, 61, and 99. The results are plotted in Figures 1 and 2 and summarized in Table II. All calculations were performed on an IBM 4381, with less CPU time required for circular chains. For a given type of molecule, calculations for large n consumed more CPU time than for small n since the upper limit of the summation index in both eq 15 and 18 increases linearly with n.

Ellipsoids of Revolution

When configurations are ellipsoids of revolution, it follows from the definitions that A_μ depends only on r and at most one angular variable. One integral is therefore

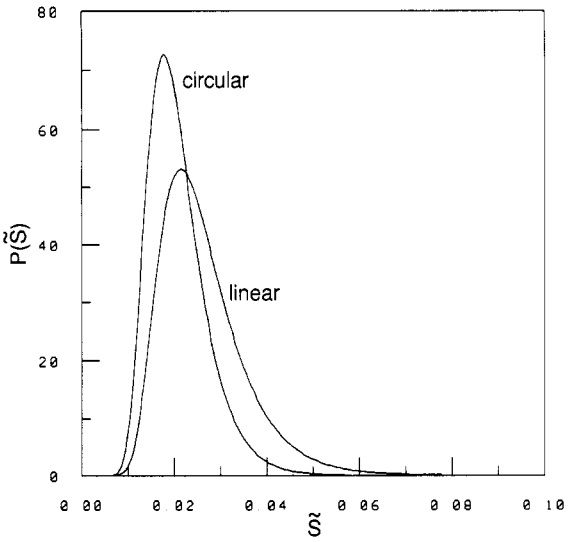

Figure 2. Distributions for 99-bead (equivalent to the large n limit) circular and linear chains as spheres.

absent from eq 8. The shape distribution is obtained on evaluation of

$$P(\tilde{S}_\parallel,\tilde{S}_\perp)\,d\tilde{S}_\parallel\,d\tilde{S}_\perp = d\tilde{S}_\parallel\,d\tilde{S}_\perp\,(4\pi/Z_2)\tilde{S}_\perp\tilde{\Delta}^2\int_{-\infty}^{\infty}dt \int_0^\infty dx \int_0^\infty dy \int_0^1 dr \int_0^{2\pi} d\alpha\, xy(x + y)F_1(t + x)F_2(t)F_3(t - y) \tag{23}$$

where $\tilde{\Delta} = \tilde{S}_\parallel - \tilde{S}_\perp$. The function $F_\mu(x)$ is the same as defined in eq 9 with $A_1 = \tilde{S}_\perp + \tilde{\Delta}(1 - r^2)\cos^2\alpha/2$, $A_2 = \tilde{S}_\perp + \tilde{\Delta}(1 - r^2)\sin^2\alpha/2$, and $A_3 = \tilde{S}_\perp + \tilde{\Delta}r^2$. We note that the α integration may be done analytically with the result expressed in terms of the Bessel function of the first kind of zero order. For present purposes, this is not done for the following reason. As in the evaluation of the distribution function for spherical configurations, we find that the expansion of the integration limits for one of the two semiinfinite integrals in eq 23 to $(-\infty, \infty)$ is also allowed (see Appendix). Therefore, by leaving the integration over **SO(3)** for the last, the improper integrals can be evaluated in ways parallel to those for spherical configurations. In the following, analytical and numerical results are obtained for linear and circular chains with an odd number of beads greater than five.

For circular chains, eq 23 is reduced to

$$P(\tilde{S}_\parallel,\tilde{S}_\perp)\,d\tilde{S}_\parallel\,d\tilde{S}_\perp = (d\tilde{S}_\parallel\,d\tilde{S}_\perp/Z_C)\tilde{S}_\perp\tilde{\Delta}^2\int_0^1\int_0^{\pi/2} dr\,d\theta \sum_{j\neq k\neq l}^{(n-1)/2}(-1)^{j+k+l}(\kappa_k - \kappa_j)(\kappa_l - \kappa_j)(\kappa_l - \kappa_k)B_jB_kB_l \times \exp(-\gamma_{jk})[\exp(-\alpha_{kl})\,\mathrm{Ei}\,(\alpha_{kl}) + \exp(-\beta_{kl})\,\mathrm{Ei}\,(\beta_{kl})] \tag{24}$$

where Z_C is a normalization constant, $\alpha_{kl} = (\kappa_l - \kappa_k)[\tilde{S}_\perp + \tilde{\Delta}(1 - r^2)\sin^2\theta]$, $\beta_{kl} = (\kappa_l - \kappa_k)[\tilde{S}_\perp + \tilde{\Delta}(1 - r^2)\cos^2\theta]$, $\gamma_{jk} = (\tilde{S}_\perp + \tilde{\Delta}r^2)\kappa_j + [2\tilde{S}_\perp + \tilde{\Delta}(1 - r^2)]\kappa_k$, and Ei (x) is the exponential-integral function. In the case of linear chains, the final equation derived from eq 23 is put into the form

$$P(\tilde{S}_\parallel,\tilde{S}_\perp)\,d\tilde{S}_\parallel\,d\tilde{S}_\perp = (d\tilde{S}_\parallel\,d\tilde{S}_\perp/Z_L)\tilde{S}_\perp\tilde{\Delta}^2\int_0^1\int_0^{\pi/2}\int_0^{\pi/2}\int_0^{\pi/2} dr\,d\alpha\,d\beta\,d\gamma \sum_{j,k=1}^{(n-1)/2}(-1)^{j+k}(\epsilon_k - \epsilon_j)D_jD_k\exp(-\omega_{jk})\{\sum_{l=k}^{(n-3)/2}(-1)^l(\epsilon_{l+1/2} - \epsilon_j)D_{l+1/2}G(\epsilon_{l+1/2} - \epsilon_k) + (-1)^{(n-1)/2}(\sigma_k + \epsilon_k - \epsilon_j)H_kG(\sigma_k)\} \tag{25}$$

where Z_L is a normalization constant, $\epsilon_j = \kappa_{2j-1} + (\kappa_{2j} - \kappa_{2j-1})$

Table III
Most Probable Configurations (Ellipsoids of Revolution)

	prolate			oblate				probability	
n	$*\tilde{S}_\parallel$	$*\tilde{S}_\perp$	$P(*\tilde{S}_\parallel,*\tilde{S}_\perp)$	$*\tilde{S}_\perp$	$*\tilde{S}_\parallel$	$P(*\tilde{S}_\parallel,*\tilde{S}_\perp)$	$\langle\tilde{S}_\parallel\rangle$	ratio	$\langle\tilde{S}_\perp\rangle$
					Circular				
5	0.0325	0.0025	982.70	0.0225	0.0025	1103.13	0.0507	2.79	0.0155
11	0.0450	0.0125	703.23	0.0275	0.0075	684.70	0.0545	2.45	0.0232
61	0.0450	0.0150	946.97	0.0275	0.0100	749.37	0.0573	3.33	0.0222
					Linear				
11	0.0700	0.0150	254.39	0.0375	0.0100	218.07	0.1287	4.77	0.0265
61	0.0725	0.0175	301.39	0.0375	0.0125	211.00	0.1346	6.31	0.0255

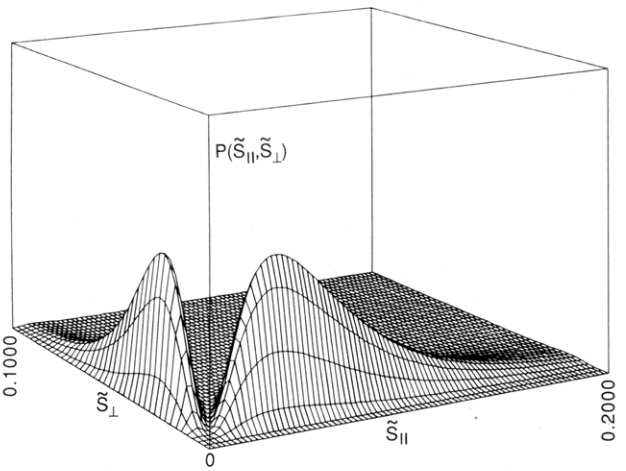

Figure 3. Shape distribution function $P(\tilde{S}_\parallel,\tilde{S}_\perp)$ for 11-bead circular chains. The reduced principal components $\tilde{S}_\mu$ of the gyration tensor are defined as $3S_\mu/2n\langle l^2\rangle_0$, where $\langle l^2\rangle_0$ is the unperturbed dimension of a segment.

$\sin^2\alpha$, D_j is the same as defined in eq 19, $\omega_{jk} = (\tilde{S}_\perp + \tilde{\Delta}r^2)\epsilon_j + [2\tilde{S}_\perp + \tilde{\Delta}(1-r^2)]\epsilon_k$, $\sigma_j = (\kappa_{n-1} - \epsilon_j)\sec^2\gamma$, and H_j and $G(x)$ are defined as

$$H_j = (\kappa_{n-1}\sigma_j)^{1/2}\sec\gamma\prod_{l=1}^{n-2}[(\sigma_j+\epsilon_j)/\kappa_l - 1]^{-1/2} \quad (26)$$

and

$$G(x) = x\exp\{-[\tilde{S}_\perp + \tilde{\Delta}(1-r^2)/2]x\}I_0[\tilde{\Delta}(1-r^2)x/2] \quad (27)$$

respectively. $I_0(x)$ is the modified Bessel function of the first kind of zero order.

As is the case for spherical configurations, the shape distribution function for five-bead circular chains is found amenable to further analytical reduction to a simple expression. The result is

$$P(\tilde{S}_\parallel,\tilde{S}_\perp)\,d\tilde{S}_\parallel\,d\tilde{S}_\perp = (d\tilde{S}_\parallel\,d\tilde{S}_\perp/C)\tilde{S}_\perp^{1/2}\tilde{\Delta}^2\times \exp(-\kappa_+\tilde{s}^2)\int_0^1 \frac{\cosh\{\kappa_-[\tilde{S}_\perp + \tilde{\Delta}(1-2\beta^2)]\}}{[\tilde{S}_\perp + \tilde{\Delta}(1-\beta^2)]^{1/2}}\,d\beta \quad (28)$$

where the normalization constant C may be written down as a simple double integral. It is also seen that the integral in eq 28 can be expressed in terms of the two-variable degenerate hypergeometric series.[22] Some numerical results obtained on evaluation of eq 28 are tabulated in Table III.

In practical numerical evaluation of eq 24 and 25, use is made of the fact that both equations can be put into the form

$$P(\tilde{S}_\parallel,\tilde{S}_\perp)\,d\tilde{S}_\parallel\,d\tilde{S}_\perp = (d\tilde{S}_\parallel\,d\tilde{S}_\perp/Z_2)\tilde{S}_\perp\tilde{\Delta}^2\int_0^1 dr\sum_{\alpha=1}^{3}G_\alpha(r)W_\alpha(r) \quad (29)$$

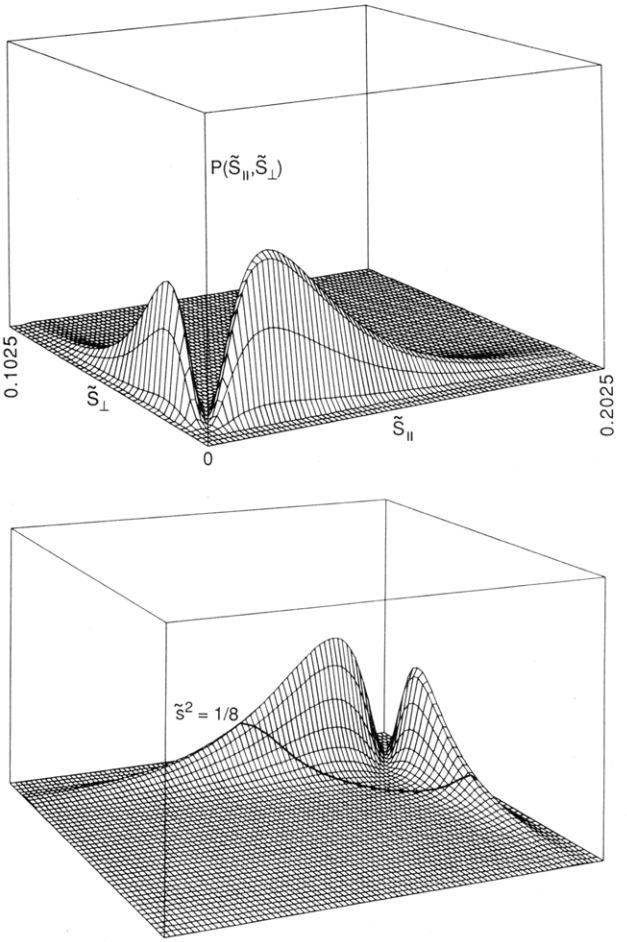

Figure 4. (Top) Shape distribution function for circular chains with $n = 61$. (Bottom) Opposite view. The heavy line depicts the mean-squared radius of gyration $\langle\tilde{s}^2\rangle_0 = {}^1/_8$ for circular chains in three dimensions.

where each component $W_\alpha(r)$ consists of, at most, one integral of a single sum and $G_\alpha(r)$ is, at most, a double integral of double sums. The last integral over r was carried out by a 10-point Gaussian quadrature[23] and those in $W_\alpha(r)$ and $G_\alpha(r)$, if any, were performed by Romberg integration.[21] The special functions $I_0(x)$ and Ei (x) were calculated with their respective IMSL function subprograms.[20] As for spheres, much more CPU time was required for computations at large n. Calculations for $n = 11$ were done on an IBM 4381 while for $n = 61$ an IBM 3090-200E was employed to do the computation. The graphical representations of $P(\tilde{S}_\parallel,\tilde{S}_\perp)$ resulting from these computations are displayed in Figures 3–6. Some numerical results are summarized in Table III.

The normalization in eq 29 is

$$Z_2 = Z_{2,p} + Z_{2,o} \quad (30)$$

where $Z_{2,p}$ and $Z_{2,o}$ are the normalization constants for

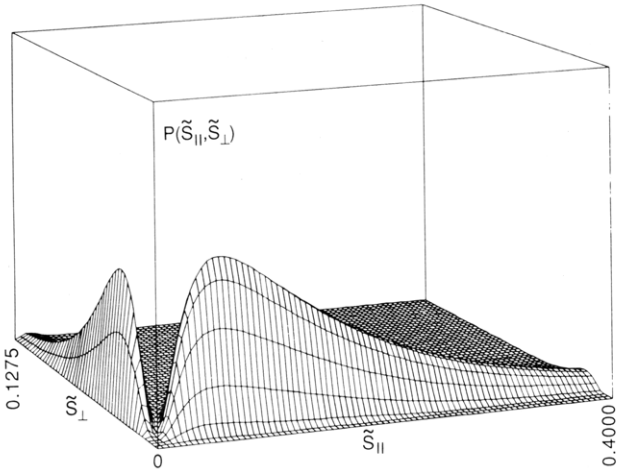

Figure 5. Distribution function for 11-bead linear chains as ellipsoids of revolution.

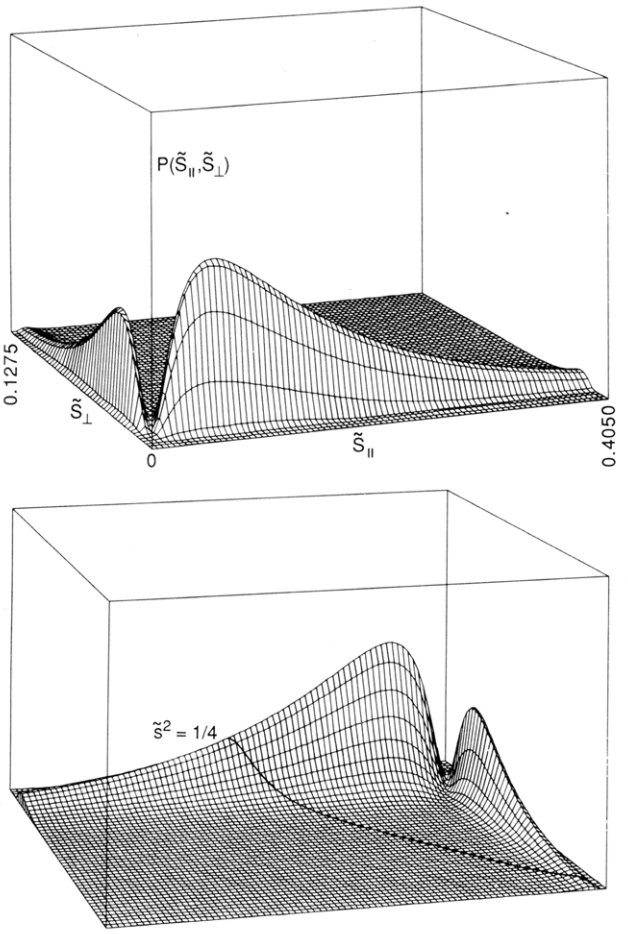

Figure 6. (Top) Distribution function for linear chains of n = 61 beads. Otherwise the same as Figure 5. (Bottom) Opposite view. The heavy curve locates the mean-squared radius of gyration, $\langle \tilde{s}^2 \rangle_0 = {}^1/_4$.

prolate ($\tilde{S}_\parallel > \tilde{S}_\perp$) and oblate ($\tilde{S}_\perp > \tilde{S}_\parallel$) ellipsoids, respectively. For prolate ellipsoids, we have

$$Z_{2,p} = \int_0^\infty d\tilde{S}_\parallel \int_0^{\tilde{S}_\parallel} d\tilde{S}_\perp \, \tilde{S}_\perp \tilde{\Delta}^2 \int_0^1 dr \sum_{\alpha=1}^{3} G_\alpha(r) W_a(r) \quad (31)$$

while for oblate ones

$$Z_{2,o} = \int_0^\infty d\tilde{S}_\perp \, \tilde{S}_\perp \int_0^{\tilde{S}_\perp} d\tilde{S}_\parallel \, \tilde{\Delta}^2 \int_0^1 dr \sum_{\alpha=1}^{3} G_\alpha(r) W_\alpha(r) \quad (32)$$

The ratio of the two, $Z_{2,p}$:$Z_{2,o}$, is the probability ratio that measures the likelihood that Gaussian molecules choose prolate configurations rather than oblate ones.

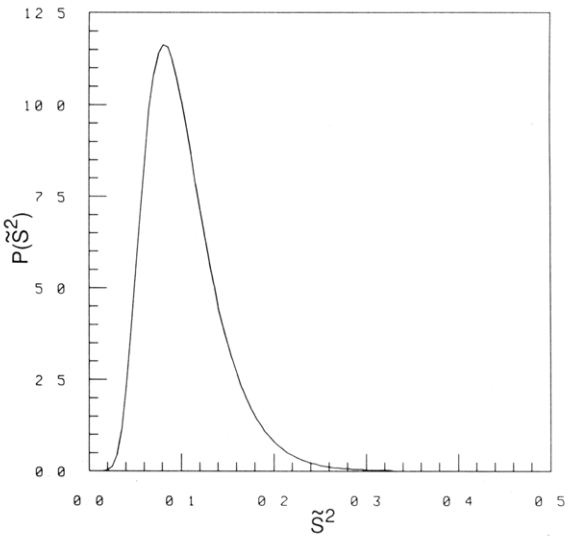

Figure 7. Distribution of the squared radius of gyration $\tilde{S}^2$ for 11-bead circular chains as ellipsoids of revolution as calculated from eq 34.

Finally, we consider a probability distribution of a quantity σ that is a linear combination of $\tilde{S}_\parallel$ and $\tilde{S}_\perp$, which may be formulated as follows:

$$P(\sigma)\, d\sigma = d\sigma \int_0^\infty \int_0^\infty \delta[\sigma - (\alpha\tilde{S}_\parallel + \beta\tilde{S}_\perp)] P(\tilde{S}_\parallel,\tilde{S}_\perp)\, d\tilde{S}_\parallel\, d\tilde{S}_\perp \quad (33)$$

For $\alpha = 1$ and $\beta = 2$, σ is simply the squared radius of gyration of the ellipsoids under consideration, which may be denoted by $\tilde{S}^2$. In this particular case, we have from eq 33

$$P(\tilde{S}^2)\, d\tilde{S}^2 = (d\tilde{S}^2/3) \int_a^b P[(\tilde{S}^2-\xi)/3,(\tilde{S}^2+2\xi)/3]\, d\xi \quad (34)$$

where $a = -\tilde{S}^2/2$ and $b = \tilde{S}^2$. A sample calculation for $P(\tilde{S}^2)$ was done for circular chains with $n = 11$. The result is plotted in Figure 7, illustrating general features of the distribution function of the radius of gyration for ellipsoids of revolution.

Discussion

The most probable spherical configurations are very compact with respect to the mean-square dimensions of general ellipsoids and even more so than their disk counterparts,[10] as is seen in Figures 1 and 2. This greater compactness of configurations in higher dimensional space may be accounted for by the greater variety of configurations as dimensionality increases. This feature also appears in the evaluation of other types of probability distributions such as those for the largest principal component.[17] As a result, spherical configurations are subject to more constraints than disks. For circular chains with $n = 99$, $*\tilde{S}$ and $\langle \tilde{S} \rangle$ are found to be 0.0175 and 0.0207, respectively, while for linear chains with the same number of beads, they are 0.0215 and 0.0261, respectively. Circular chains are thus seen to be less extended than linear chains, as expected. Limiting distributions for large n for both circular and linear chains are rapidly reached as n passes aproximately 50.

The probability of finding spheres in the configuration space of ellipsoids of revolution is zero. This is also seen in the defining equations, eq 5 and 6, for the shape distribution functions. The consequence of this fact is seen in Figure 3–6; the two parts of the distribution are separated by a vertical plane that cuts the space on the line $\tilde{S}_\parallel = \tilde{S}_\perp$ on the zero-probability-density plane. The part

representing the distribution for prolate ellipsoids of revolution is restricted by the inequality $\tilde{S}_\parallel > \tilde{S}_\perp$. Similarly, the part belonging to oblate ones is constrained by $\tilde{S}_\parallel < \tilde{S}_\perp$. In figure 3, $P(\tilde{S}_\parallel,\tilde{S}_\perp)$ for circular chains with $n = 11$ is plotted against $\tilde{S}_\parallel$ and $\tilde{S}_\perp$ with the same grid size (0.0025) for both axes. As is seen, the larger volume of the prolate part indicates that these chains are more likely to be prolate than oblate. This turns out to be true in general for both circular and linear chains as is observed in Figures 4–6. From Table III, the most probable dimensions for 11-bead circular chains, $^*\tilde{S}_\parallel$ and $^*\tilde{S}_\perp$, in the prolate region are 0.0450 and 0.0125, respectively, as opposed to the corresponding values, 0.0075 and 0.0275, for oblate ellipsoids of revolution. The larger value for the probability density at the most probable configuration in the prolate region for circular chains with $n = 11$ implies that their most probable configurations are prolate ellipsoids of revolution. The opposite is true for five-bead circular chains. Similar features are found for larger n circular chains and linear chains. Within the prolate or oblate region, however, the general features exhibited by these distributions are similar to those in two dimensions.[10] This includes the long tails of the distributions as the larger component becomes large and the fact that the fluctuations away from the most probable configurations are highly asymmetric. Figure 5 displays the linear chain counterpart of Figure 3, which exhibits, in addition to what the latter reveals, even longer tails in the distributions. Figures 4 and 6 represent large n-limiting distributions. Each is presented with both front and back views displayed. For $n = 61$, linear chains have $^*\tilde{S}_\parallel = 0.0725$ and $^*\tilde{S}_\perp = 0.0175$ with $^*\tilde{s}^2$ being only 43% of the mean-square radius of gyration, $\langle\tilde{s}^2\rangle_0 = {}^1/_4$. For circular chains, $^*\tilde{s}^2$ is 60% of $\langle\tilde{s}^2\rangle_0 = {}^1/_8$. Both the most probable and average dimensions of linear chains are larger than those for circular chains, as seen in Table III, which stands to reason. It is found that the ratio $^*\tilde{S}_\parallel{:}^*\tilde{S}_\perp$ for both prolate and oblate ellipsoids of revolution rapidly reaches its limiting value as n increases for both linear and circular chains.

Finally, we note that the numerically computed quantity $\langle\tilde{S}_\parallel\rangle + 2\langle\tilde{S}_\perp\rangle$ for circular and linear chains with $n = 61$ is 0.1017 and 0.1856, respectively. These values are 81% and 74% of their respective $\langle\tilde{s}^2\rangle_0$. This feature may be better appreciated in Figure 7, which shows the distribution function for $\tilde{S}^2$ for the 11-bead circular chain on the subspace of ellipsoids of revolution. It must be noted that the distribution under consideration is different from that commonly referred as the distribution of the radius of gyration, which is formulated in the complete configuration space.

Acknowledgment. This work was supported by Department of Energy through Grant DE-FG06-84ER45123. We thank both the IBM Corporation for a materials science grant leading to acquisition of an IBM4381 and the University of Washington for allocating computing time on its IBM3090-200E.

Appendix. Proofs of Extension and Reduction of Integration Limits in 3-D Shape Distribution Functions

Denote the integral part of the 3-D shape distribution function defined in eq 6 by $I(\tilde{\mathbf{S}}_d)$ and make a change of variables to $t = (x_1 + x_2 + x_3)/3$, $x = (x_1 - x_2)/3$ and $y = (x_2 - x_3)/3$. The function $I(\tilde{\mathbf{S}}_d)$ may then be written as

$$I(\tilde{\mathbf{S}}_d) = \int_{-\infty}^{\infty}dt \int_0^{\infty}dx \int_0^{\infty}dy\, xy(x+y)\exp(i\tilde{s}^2t) \times W(x,y)D(t+2x+y)D(t-x+y)D(t-x-2y) \quad \text{(A-1)}$$

where $D(x) = \prod_{j=1}^{n-1}(\kappa_j + ix)^{-1/2}$ and $W(x,y)$ is given by

$$W(x,y) = \exp(-i\ \mathrm{tr}\ \mathbf{A}\ \mathrm{tr}\ \mathbf{B}) \int_{\mathbf{so(3)}} \mathrm{etr}\ (i3\mathbf{AhBh}')\ \mathbf{dh} \quad \text{(A-2)}$$

where $\mathbf{A} = \mathrm{diag}\ (\tilde{S}_1{-}\tilde{S}_3, \tilde{S}_2{-}\tilde{S}_3, 0)$ and $\mathbf{B} = \mathrm{diag}\ (x{+}y, y, 0)$. Now let $z = t - x + y$. Equation A-1 may then be transformed to

$$I(\tilde{\mathbf{S}}_d) = \int_{-\infty}^{\infty}dz \int_0^{\infty}dx \int_0^{\infty}dy\, D(z)\exp(i\tilde{s}^2z)xy(x+y)W(x,y)U(x)U(-y) \quad \text{(A-3)}$$

where $U(x)$ is defined as

$$U(x) = D(z+3x)\exp(i\tilde{s}^2x) \quad \text{(A-4)}$$

In what follows, a key relation for $W(x,y)$ is first derived, from which follows two desired proofs.

1. Proof that $W(\mathbf{x},\mathbf{y}) = \overline{W(\mathbf{y},\mathbf{x})}$. Let us first consider

$$F(x_1,x_2,x_3) = \int_{\mathbf{so(3)}} \mathrm{etr}\ (i\mathbf{ahxh}')\ \mathbf{dh} \quad \text{(A-5)}$$

where $\mathbf{a} = \mathrm{diag}\ (\tilde{S}_1,\tilde{S}_2,\tilde{S}_3)$ and $\mathbf{x} = \mathrm{diag}\ (x_1,x_2,x_3)$. It then follows from the properties of $\mathbf{SO(3)}$ that

$$F(x_1,x_2,x_3) = F(x_3,x_2,x_1) \quad \text{(A-6)}$$

By definition (see eq 6 and A-1), we have

$$F(x_1,x_2,x_3) = \exp(i\tilde{s}^2t)W(x,y) \quad \text{(A-7)}$$

Now consider

$$F(x_3,x_2,x_1) = \exp(i\tilde{s}^2t)G(x,y) \quad \text{(A-8)}$$

where $G(x,y)$ is given by

$$G(x,y) = \exp(i\ \mathrm{tr}\ \mathbf{A}\ \mathrm{tr}\ \mathbf{C}) \int_{\mathbf{so(3)}} \mathrm{etr}\ (-i3\mathbf{AhCh}')\ \mathbf{dh} \quad \text{(A-9)}$$

in which $C = \mathrm{diag}\ (y{+}x, x, 0)$. We note that $G(x,y) = \overline{W(y,x)} = W(-y,-x)$. Therefore, by equating eq A-7 and eq A-8, we complete the proof.

2. Proof of Extension and Reduction of Integration Limits. We note that the proof of extension of the integration limits is equivalent to proving that

$$\int_0^{\infty}dx \int_{-\infty}^{0}dy\, xy(x+y)W(x,y)U(x)U(-y) = 0 \quad \text{(A-10)}$$

To verify eq A-10, rewrite it in the form

$$\int_0^{\infty}dx \int_0^{\infty}dy\, xy(x-y)W(x,-y)U(x)U(y) = 0 \quad \text{(A-11)}$$

which is readily proved by using the symmetry relation for $W(x,y)$ derived earlier.

Similarly, to give a proof of reduction of the integration limits, we first verify the relation

$$\int_{-\infty}^{0}R(z,x,y)\,dz = \int_0^{\infty}\overline{R(z,y,x)}\,dz \quad \text{(A-12)}$$

where $R(z,x,y)$ is defined as

$$R(z,x,y) = D(z)\exp(i\tilde{s}^2z)W(x,y)U(x)U(-y) \quad \text{(A-13)}$$

Equation A-12 is easily proved by noting that $D(-x) = \overline{D(x)}$ and $W(x,y) = \overline{W(y,x)}$. It then follows immediately that

$$I(\tilde{\mathbf{S}}_d) = 2\ \mathrm{Re} \int_0^{\infty}dz \int_0^{\infty}dx \int_0^{\infty}dy\, D(z)\exp(i\tilde{s}^2z)xy(x+y)W(x,y)U(x)U(-y) \quad \text{(A-14)}$$

Equations A-10 and A-14 complete the proofs.

References and Notes

(1) Eichinger, B. E. *Macromolecules* **1972**, *5*, 496.
(2) Eichinger, B. E. *Pure Appl. Chem.* **1975**, *43*, 97.
(3) Šolc, K.; Stockmayer, W. H. *J. Chem. Phys.* **1971**, *54*, 2756.

(4) Šolc, K. *J. Chem. Phys.* **1971**, *55*, 335.
(5) Šolc, K.; Gobush, W. *Macromolecules* **1974**, *7*, 814.
(6) Stockmayer, W. H. *XXIVth International Congress of Pure and Applied Chemistry*; Butterworths: London, 1974; Vol. 1, p 91, and references therein.
(7) Eichinger, B. E. *Macromolecules* **1977**, *10*, 671.
(8) Eichinger, B. E. *Macromolecules* **1985**, *18*, 211.
(9) Muirhead, R. J. *Aspects of Multivariate Statistical Theory*; Wiley: New York, 1982; Chapter 7.
(10) Shy, L. Y.; Eichinger, B. E. *Macromolecules* **1986**, *19*, 838.
(11) Theodorou, D. N.; Suter, U. W. *Macromolecules* **1985**, *18*, 1206.
(12) Bishop, M.; Saltiel, C. J. *J. Chem. Phys.* **1986**, *85*, 6728.
(13) Aronovitz, J. A.; Nelson, D. R. *J. Phys. (Les Ulis, Fr.)* **1986**, *47*, 1445.
(14) Rudnick, J.; Gaspari, G. *Science* **1987**, *237*, 384.
(15) Rudnick, J.; Beldjenna, A.; Gaspari, G. *J. Phys. A: Math. Gen.* **1987**, *20*, 971.
(16) Gaspari, G.; Rudnick, J.; Beldjenna, A. *J. Phys. A: Math. Gen.* **1987**, *20*, 3393.
(17) Bishop, M.; Saltiel, C. J. *J. Chem. Phys.* **1988**, *88*, 3976.
(18) Abramowitz, M.; Stegun, I. A. *Handbook of Mathematical Functions*; National Bureau of Standards: Bethesda, 1970; *Applied Math. Sec. 55*, p 230.
(19) Coriell, S. R.; Jackson, J. L. *J. Math. Phys.* **1967**, *8*, 1276.
(20) *The IMSL Library, Reference Manual*, 9th ed.; International Mathematical and Statistical Libraries: Houston, TX, 1982; Programs MMDEI and MMBSIO.
(21) Gerald, C. F. *Applied Numerical Analysis*, 3rd ed.; Addison Wesley: Reading, MA, 1984; Chapter 4.
(22) Gradshteyn, I. S.; Ryzhik, I. M. *Table of Integrals, Series, and Products*; Academic Press: New York, 1965: Entry 8.212.6, p 925; Entry 9.261.1, p 1067.
(23) Press, W. H.; Flannery, B. P.; Teukolsky, S. A.; Vetterling, W. T. *Numerical Recipes*; Cambridge University Press: Cambridge, New York, 1986; Chapter 4.

Interpretation of Long-Chain Structure in Flexible Homopolymers from Dilute-Solution Dynamic Properties Measured in Good Solvents

Robert L. Sammler† and John L. Schrag*

Department of Chemistry and Rheology Research Center, University of Wisconsin, Madison, Wisconsin 53706. *Received September 16, 1988; Revised Manuscript Received January 27, 1989*

ABSTRACT: Non-Gaussian effects on the frequency dependence of intrinsic birefringence or intrinsic viscoelasticity are investigated for flexible homopolymers in dilute solution. The effects are examined for bead–spring model chains having linear or regular star geometry by using the approximate framework of Ptitsyn and Eizner. Predicted properties are computed for chains of finite size for both uniform and nonuniform chain expansions; the results are compared to those of the Gaussian model. These comparisons clarify why measured dynamic properties of flexible homopolymers dissolved in good solvents often correspond quantitatively to properties computed for the Gaussian model. Long-chain structure parameters obtained by fitting measured dynamic properties with Gaussian model predictions are expected to be at most weakly dependent on solvent power.

I. Introduction

The frequency dependence of the modified intrinsic birefringence $[S^*]_\Delta$ and viscoelasticity $[\eta^*]_\Delta$ has recently[1] been shown to have excellent potential for characterization of long-chain structure in monodisperse samples of flexible homopolymers. However, these low-shear-rate predictions were based on a Gaussian chain model that makes them most applicable to measured properties of homopolymers in Θ solvents. Properties in Θ solvents—especially required to characterize long-chain structure—are particularly difficult to obtain relative to those in good solvents; the signals are lower and the accessible effective frequency range is much smaller since time–temperature superposition techniques[2] are no longer applicable. Properties in Θ solvents are also less sensitive to long-chain structure because the breadth of the relaxation time spectrum characterizing the conformational motions of a chain in solution compresses as the solvent power diminishes. These concerns make the measurement of solution properties in good solvents much more attractive, though the interpretation of long-chain structure from such properties is complicated by the lack of a rigorous, mathematically tractable theory quantitatively predicting these properties for non-Gaussian chains. Fortunately, as summarized in ref 1, the Gaussian model has been surprisingly successful in fitting properties measured in good solvents; this has been done by experimentalists for at least 20 years.[2] Strictly speaking, the interpretation of the fit parameters has not been entirely clear because of the non-Gaussian nature of the real chains; our purpose here is to investigate non-Gaussian effects on the fit parameters. Non-Gaussian effects are predicted with the bead–spring model formulated in the approximate framework of Ptitsyn and Eizner;[3-5] chains of finite size and various degrees of hydrodynamic interaction are considered. These predictions are then fit by those of the Gaussian bead–spring model. Differences in the (Gaussian chain) fit parameters relative to those used to generate the non-Gaussian properties are discussed. Only linear chains and regular stars are investigated; the results for other geometries are expected to be intermediate to these cases.

II. The Ptitsyn–Eizner Prescription

The Gaussian bead–spring model was first modified to include non-Gaussian effects (linear chains) by Ptitsyn and Eizner.[3-5] Since then their approach has been employed by Tschoegl,[6] Bloomfield and Zimm,[7] and Bloomfield and Sharp[8] to investigate low-frequency viscoelastic (VE) properties of infinitely long linear chains, rings, and regular stars. The justification for their approximate corrections

†Current address: Polymer Products Department, E. I. du Pont de Nemours and Co., Inc., PO Box 80269, Wilmington, DE 19880-0269.

0024-9297/89/2222-3435$01.50/0